PHYSICAL REVIEW D **88,** 074507 (2013)

SU(3) deconfining phase transition with finite volume corrections due to a confined exterior

Bernd A. Berg and Hao Wu

Department of Physics, Florida State University, Tallahassee, Florida 32306-4350, USA

(Received 6 June 2013; published 25 October 2013)

Using the geometry of a double-layered torus, we investigate the deconfining phase transition of pure SU(3) lattice gauge theory by Markov chain Monte Carlo simulations. In one layer, called "outside," the temperature is set below the deconfining temperature and in the other, called "inside," it is iterated to a pseudotransition temperature. Lattice sizes are chosen in a range suggested by the physical volumes achieved in relativistic heavy ion collisions, and both temperatures are kept close enough to stay in the SU(3) scaling region, which is required for approaching a quantum continuum limit. Properties of the transition are studied as a function of the volume for three outside temperatures. When compared with infinite volume extrapolations, small volume corrections of the deconfining temperature and width compete with those found by including quarks. Effective finite-size scaling exponents of the specific heat and Polyakov loop susceptibilities are also calculated.

DOI: 10.1103/PhysRevD.88.074507 PACS numbers: 11.15.Ha, 12.38.Mh, 25.75.Nq, 64.60.an

I. INTRODUCTION

Experimentally, the deconfining phase transition has been studied in heavy ion scattering experiments, notably at the relativistic heavy ion collider (RHIC) of Brookhaven National Lab and at the LHC at CERN. Inevitably a quark gluon plasma phase created in a laboratory experiment is limited to a small hot volume, which is surrounded by a cold exterior. These volumes are not of a fixed size, but one has to deal with data from an ensemble of differently sized volumes created by central and less central collisions. For instance, at the RHIC one scatters Au atoms, and the dimension in transverse direction is limited by the radius of the Au nucleus, which is about 6.5 fm when one calculates it from the formula [1] $R = r_0 A^{1/3}$, where $r_0 = 1.5$ fm and A is the mass number. In the longitudinal direction the Au nuclei are Lorentz contracted so that this extension of the plasma becomes set by the speed of light times the expansion time after a binary collision. For example, an expansion time of 10^{-23} s would give a longitudinal extension of 3 fm. Volumes of quark gluon plasma fireballs from sufficiently central collisions range then from 5–10 fm in the transverse as well as in the longitudinal directions. See, for instance, Ref. [2] for a figure of the density distribution. There has been and still is some debate whether such a plasma will equilibrate in the available time. This is not the subject of this paper, which relies on equlibrated configurations from Markov chain Monte Carlo (MCMC) simulations.

MCMC calculations for lattice gauge theory (LGT) provide theoretical estimates for thermodynamic quantities of the deconfining phase transition, in particular for the temperature and width. In contrast to the physical situation of heavy ion collisions, simulations of the transition focused on the infinite volume limit in which boundary effects become negligible. Notable exceptions are provided by some older work [3] and more recent investigations of finite volume effects for pure SU(3) lattice gauge theory [4,5], for QCD [6–8] and for a Polyakov-Nambu-Jona-Lasinio model [9].

Most LGT calculations use periodic boundary conditions (PBC), because they ensure a fast approach to the infinite volume limit. But they are not suitable when one wants to study the effect of an exterior confined phase on a small volume, which is deconfined or at the transition temperature. In previous work [4] on $N_\tau N_s^3$ lattices, zero outside temperature was targeted and modeled by the strong coupling limit $\beta \to 0$ (i.e., lattice spacing $a(\beta) \to \infty$) on plaquettes crossing the boundary and called cold boundary condition (CBC). For illustrative purposes, physical dimensions of the N_s^3 space volumes were calculated by assuming for the infinite volume deconfining temperature the value $T_t^\infty = 174$ MeV, which is in the range of QCD estimates obtained from LGT calculations (results reported in a recent review [10] range from 147 to 192 MeV). The value $T_t^\infty = 174$ MeV corresponds to a temporal lattice size $L_\tau = a(\beta)N_s = 1/T_t^\infty$ of approximately $L_\tau = 1.1$ fm. With this scale, spatial dimensions $L_s = a(\beta)N_s$ were set in the range 4 fm $< L_s <$ 12 fm. Thus they are realistically sized with respect to RHIC experiments, and one can investigate questions about the size of boundary effects. For volumes from 12 down to 7 fm, an increase of the effective deconfining temperature from 10 to 30 MeV was computed with a diverging trend up to 90 MeV when L_s was reduced down to 4 fm. These are sizeable corrections, though the composition of the experimental ensemble of deconfined volumes into which the LGT results ought to enter remains to be analyzed.

A theoretical shortcoming of CBCs is that they do not allow for a joint (quantum) continuum limit of the inside and outside volumes, because the construction mixes an inside SU(3) scaling region with a strong coupling limit. Although agreement with SU(3) scaling was seen for the (inside) pseudotransition temperatures and widths when

 © 2013 American Physical Society

varying the temporal lattice extension N_τ from 4 to 6, one may still be worried. Building on [4], the aim of our paper is to calculate for pure SU(3) lattice gauge theory effects due to relatively small temperature differences at the boundaries, so that both volumes can be kept in the SU(3) scaling region, which allows in principle for a joint quantum continuum limit. The penalty is that outside and inside temperatures are then rather close. Our aim is to show that even within such limits, corrections to the infinite volume extrapolations are visible, supporting that CBCs give reasonable results. In this sense the present investigation supplements the CBC calculations.

We use the Wilson action [11] on a four-dimensional hypercubic lattice. Configurations are weighted with a Boltzmann factor $\exp[S(\{U\})]$, where

$$S(\{U\}) = \sum_{\square} \beta_{\square} S_{\square}, \quad S_{\square} = \frac{1}{3}\mathrm{Re}(U_{i_1 j_1} U_{j_1 i_2} U_{i_2 j_2} U_{j_2 i_1}). \quad (1)$$

Here i_1, j_1, i_2, and j_2 label the sites circulating about the square $\square$ and the U_{ij} are SU(3) matrices. For later convenience, we allow the coupling constant,

$$g^2_{\square} = 6/\beta_{\square}, \quad (2)$$

to depend on the position of the plaquette.

Numerical evidence supports that SU(3) lattice gauge theory with the Wilson action (1) exhibits for infinite volumes a weak first-order [12] deconfining phase transition at pseudotransition coupling constant values $\beta_t^\infty(N_\tau) = 6/g_t^2(N_\tau)$. In this paper we set the scale in our calculations by the corresponding SU(3) deconfining transition temperature T_{t}^∞ and report results as a function of the reduced temperature,

$$t = \frac{T - T_{\mathrm{t}}^\infty}{T_{\mathrm{t}}^\infty}. \quad (3)$$

This allows one to confront results with dynamical quark calculations without assuming a MeV value for the transition temperature T_{t}^∞.

To make sure that the encountered corrections are not strong coupling artifacts, we consider in the present paper differences between inside and outside temperature that are small enough to keep both regions in the SU(3) scaling region so that a common continuum limit becomes, in principle, possible. Reduced outside temperatures t_{out} in the confined region are taken close to

$$t_1 = -0.095, \qquad t_2 = -0.073 \quad \text{and} \quad t_3 = -0.036, \quad (4)$$

i.e., only about 10% into the direction of the desired limit $t \to -1$. Inside temperatures are then iterated to pseudotransition values, which we locate by maxima of the SU(3) Polyakov loop susceptibility. A possible geometry would use for the inside a $N_\tau n_s^3$ sublattice of a $N_\tau N_s^3$ lattice with PBC ($n_s < N_s$). We decided instead to explore the interesting geometry of a double-layered torus (DLT), which joins two $N_\tau N_s^3$ lattices so that each N_s^3 volume provides the boundary of the other [5].

One would like to repeat these calculations for lower and lower values of t_{out} to study the approach to -1, while staying in the SU(3) scaling region. In practice this is impossible, because prohibitively large lattices would be required. However, it appears reasonable to assume that the pseudotransition inside temperatures and widths increase monotonically for a decreasing outside temperature. Therefore, finding this effect for the t_{out} values (4) and their approach towards results from the outside approximation by a strong coupling region gives us increased confidence in physical relevance of the CBC approach.

In the next section we give details of the DLT construction. For subsequent reference we present in Sec. III simulations on lattices with PBC after introducing our observables and the lambda lattice scale of Ref. [13], which we use for our analysis. Within the DLT geometry, finite volume corrections to the SU(3) deconfining transition are studied in Sec. IV. In addition to our main focus, we add in Sec. V a discussion of the finite-size scaling exponents of the specific heat and our Polyakov loop susceptibilities for large spatial lattices. Summary and conclusions follow in Sec. VI. All MCMC simulations for this paper were performed with the SU(3) FORTRAN programs, which we documented in Ref. [14].

II. DOUBLE-LAYERED TORUS

The DLT [5] extends PBC by using two layers. Let us first recall the definition of PBC for a lattice of size $\prod_{i=1}^4 N_i$. We label its sites by integer four-vectors,

$$n = (n_1, n_2, n_3, n_4),$$

with coordinates $n_i = 0, \ldots, N_i - 1$ $(i = 1, \ldots, 4)$. Steps in forward direction are defined by

$$n_i \oplus 1 = \begin{cases} n_i + 1 & \text{for } n_i < N_i - 1, \\ 0 & \text{for } n_i = N_i - 1, \end{cases} \quad (5)$$

and steps in backward direction by

$$n_i \ominus 1 = \begin{cases} n_i - 1 & \text{for } n_i > 0, \\ N_i - 1 & \text{for } n_i = 0. \end{cases} \quad (6)$$

Our DLT is defined by two identical lattices of size $N_\tau N_s^3$. We label their coordinates by n_i^ℓ, $\ell = 0, 1$. PBC are used in the temporal $(i = 4)$ direction. Defining

$$\ell' = \mathrm{mod}(\ell + 1, 2) = \begin{cases} 1 & \text{for } \ell = 0, \\ 0 & \text{for } \ell = 1, \end{cases} \quad (7)$$

the DLT boundary conditions (BCs)in the space directions $(i = 1, 2, 3)$ are for steps in forward direction,

$$n_i^\ell \oplus 1 = \begin{cases} [n_i + 1]^\ell & \text{for } n_i^\ell < N_i - 1, \\ 0^{\ell'} & \text{for } n_i^\ell = N_i - 1, \end{cases} \quad (8)$$

and for steps in backward direction,

$$n_i^\ell \ominus 1 = \begin{cases} [n_i - 1]^\ell & \text{for } n_i^\ell > 0, \\ [N_i - 1]^{\ell'} & \text{for } n_i^\ell = 0. \end{cases} \quad (9)$$

The other layer is entered whenever the same lattice would be entered from the other side in case of PBC. For two space dimensions, the topology is that of a Klein bottle.

The usual derivation, for instance [15], of the interpretation of the inverse temporal lattice extension (in which we have PBC) is still valid and we find for equilibrium configurations

$$T = \frac{1}{a(\beta_\ell) N_\tau} \quad (10)$$

for the physical temperature. Here we allow distinct coupling constants β_0 and β_1 for the layers [in LGT β is defined by (2) and not $1/(kT)$]. As for the action in Eqs. (1) and (2), coupling constants are assigned to entire plaquettes. SU(3) matrices in Eq. (1) are defined on directed links, which originate from sites of the layers and point forward in one of the four directions (a matrix U is replaced by U^{-1} when it is encountered in reverse direction of the link). Our rule is that we use the coupling constant value β_1 for a plaquette if any of its links originate in the $\ell = 1$ layer. Otherwise, the value β_0 is used. This introduces a slight asymmetry for their assignments in our two layers. The $\ell = 0$ layer will be taken as the outside and the $\ell = 1$ layer as the inside volume.

The MCMC process equilibrates the entire system by providing for each SU(3) matrix the appropriate infinite heat bath reservoir. Distinct couplings in different regions are no obstacle and are used as well in other systems such as spin glasses. In the infinite volume limit, each layer equilibrates at its own temperature and the other layer serves as boundary. At the boundaries a quasistatic region emerges with a temperature gradient from one into the other. For small finite volumes, effects from this boundary region are not negligible.

III. DECONFINING TRANSITION WITH PBC

First, we define the observables used in this paper. Subsequently, the SU(3) lambda lattice scale of Ref. [13] is introduced. Finally in this section, we present our MCMC simulations with PBC. Each data point relies on 2^{13} sweeps for reaching equilibrium and thereafter 64×2^{13} measurements, each separated from the next by 4 sweeps. Error bars (given in parentheses) were calculated with respect to jackknife bins, so that autocorrelations are properly accounted for. For most data sets it was possible to use 32 or more jackknife bins, so that the statistical interpretation of these error bars is up to two standard deviations practically Gaussian according to their Student distribution. See, for instance, Ref. [16] for the underlying statistics. Details about the autocorrelations of our data can be found in [17]. Improved estimators relying on the multihit approach [18] were explored, but found rather inefficient in our range of coupling constant values, and the simulations remained very CPU time demanding.

A. Observables

The specific heat of the LGT system is

$$C(\beta) = \frac{1}{6N}[\langle S^2 \rangle - \langle S \rangle^2], \quad (11)$$

where N is the total number of lattice sites. Writing the sum over all Polyakov loops on the lattice as

$$P = \sum_{\vec{x}} P_{\vec{x}}, \quad (12)$$

the magnetic Polyakov loop susceptibility is defined by

$$\chi = \frac{1}{N_{\vec{x}}}[\langle |P|^2 \rangle - \langle |P| \rangle^2], \quad (13)$$

and the thermal Polyakov loop susceptibility by

$$\chi^\beta = \frac{1}{N_{\vec{x}}} \frac{d}{d\beta} \langle |P| \rangle^2, \quad (14)$$

where $N_{\vec{x}}$ is the total number of spatial lattice sites, $N_{\vec{x}} = N_s^3$ in our geometry.

As signal for the pseudotransition temperature, we use in this paper the locations of the maxima of the magnetic Polyakov loop susceptibility and drop the adverb "magnetic." For $N_\tau = 4$ the curves are shown in Fig. 1. For smaller lattices, the yellow line for $N_s = 20$ and the two lines below, the curves are almost flat on the β range of the figure. If the range is sufficiently extended, they are also clearly peaked. The thermal Polyakov loop susceptibility gives, slightly shifted, similarly strong signals, whereas the maxima of the specific heat are less pronounced.

Another interesting quantity is the structure factor (see, e.g., Refs. [19,20]),

$$F(\vec{k}) = \frac{1}{N_{\vec{x}}} \left\langle \left| \sum_{\vec{x}} P_{\vec{x}} \exp(i\vec{k}\vec{x}) \right|^2 \right\rangle, \qquad \vec{k} = \frac{2\pi}{N_s} \vec{n}, \quad (15)$$

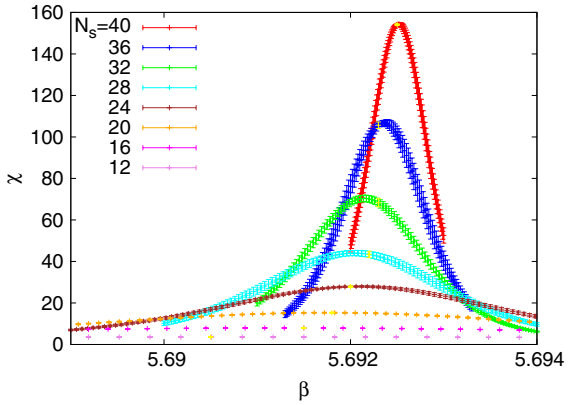

FIG. 1 (color online). Reweighted Polyakov loop magnetic susceptibilities for $N_\tau = 4$ PBC lattices. The ordering in the legend agrees with that of the curves.

where $\vec{n}$ is an integer vector. These quantities are important in the determination of finite-size scaling exponents. Specifically, for large spatial dimension N_s, the maxima of the above quantities scale like

$$C_{\max} = C(\beta_{\max}) \sim N_s^{\alpha/\nu}, \tag{16}$$

$$\chi_{\max} = \chi(\beta_{\max}) \sim N_s^{\gamma/\nu}, \tag{17}$$

$$\chi^{\beta}_{\max} = \chi^{\beta}(\beta_{\max}) \sim N_s^{(1-\beta)/\nu}, \tag{18}$$

$$F_{\max}(\vec{k}) = F(\vec{k};\beta_{\max}) \sim N_s^{2-\eta}. \tag{19}$$

Definitions of the exponents α, β, γ, ν, η and finite-size scaling relations can be found in [21]. For a first-order transition we have

$$\nu = \frac{1}{D}, \qquad \frac{\alpha}{\nu} = D, \qquad \frac{\gamma}{\nu} = D, \qquad \frac{1-\beta}{\nu} = D, \tag{20}$$

where D is the dimension of the spatial volume of the system under study.

For η the situation of a first-order transition is that one has a superposition of the disordered phase, where $\eta = 2$ holds, and the ordered phase with $\eta = 2 - D$ (at the critical point of a second-order transition two-point correlation falloff like $|\vec{r}|^{-D+2-\eta}$). This limits the usefulness of structure factors for equilibrium investigations of first-order transitions, while they played some role in an investigation of the dynamics of the SU(3) deconfining transition [20]. As we have calculated $F(\vec{k})$ for the smallest momenta, $\vec{k} = (2\pi/N_s, 0, 0)$ and cyclic permutations thereof, we report maxima $F_{\max}$ of this quantity together with maxima for our other observables.

B. SU(3) scaling

Like any mass in pure SU(3) LGT, the temperature is in the quantum continuum limit related by a constant to the lambda lattice scale Λ_L,

$$T = \frac{1}{a(\beta)N_\tau} = \frac{1}{L_\tau} = c_T \Lambda_L. \tag{21}$$

Using accurate MCMC data for the potential of a static quark-antiquark pair, an effective nonperturbative parametrization of the lambda lattice scale was derived by Necco and Sommer [13] for the range $5.7 \le \beta \le 6.92$,

$$a\Lambda_L = f_\lambda(\beta) = \text{const}\exp[-1.6804 - 1.7331(\beta-6) + 0.7849(\beta-6)^2 - 0.4428(\beta-6)^3], \tag{22}$$

which we adopt for our analysis. In the scaling window of a lattice of fixed size, we have for the coupling constant ($g^2 = 6/\beta$) dependence of the reduced temperature,

$$t(\beta) = \frac{f_\lambda(\beta_t^\infty)}{f_\lambda(\beta)} - 1. \tag{23}$$

Notably, the constant in the definition (22) of the lambda lattice scale drops out.

C. Numerical results

In this section we report from our simulations with PBC. The results are summarized in Tables I and II. They rely on reweighting [22,23]. For each lattice size, a time series from a single simulation point β_0 turns out to be sufficient. The values of β_0 are given in Table I. As there are few finite-size effects with PBC, it is easy to estimate appropriate β_0 values in advance from previous simulations on smaller lattices, so that the pseudotransition couplings β_t in the next column of Table I are well within the reweighting range. Following [23] (compare figures 1 and 3 of this paper), we define the reweighting range in β by q tiles s_q and s_{1-q} of the action times series and the requirement that the reweighted action average $\bar{s}(\beta)$ has to lie in between these q tiles, $s_q < \bar{s}(\beta) < s_{1-q}$. Even when generous 10% q tiles are used, all β_t values are found well within this range. For $N_\tau = 4$ the underlying reweighted Polyakov loop susceptibilities are shown in Fig. 1.

Below the pseudotransition couplings β_t in Table I, their infinite volume extrapolations β_t^∞ are listed, relying on fits with const$/N_s^3$ corrections. Using them and Eq. (23), the reduced temperatures $t(\beta_t)$ are found as listed in the next column of Table I. Their error bars are calculated by standard error propagation for independent events, which

TABLE I. PBC: Pseudo-transition coupling constant values, reduced temperatures and widths.

$N_\tau N_s^3$	β_0	β_t	t	$\triangle\beta_t^{4/5}$
412^3	5.6905	5.69055 (21)	−0.00449 (50)	0.01452 (17)
416^3	5.6910	5.69124 (16)	−0.00288 (39)	0.00666 (11)
420^3	5.6918	5.69175 (12)	−0.00168 (30)	0.003547 (73)
424^3	5.6920	5.69210 (14)	−0.00086 (34)	0.002015 (43)
428^3	5.6922	5.69226 (10)	−0.00049 (25)	0.001261 (20)
432^3	5.6923	5.69215 (07)	−0.00075 (19)	0.0008432 (96)
436^3	5.6924	5.69236 (07)	−0.00026 (19)	0.0005753 (70)
440^3	5.6925	5.69252 (05)	+0.00012 (15)	0.0004088 (26)
4∞	⋯	5.692469 (42)	0.00000 (10)	0
624^3	5.8934	5.89368 (34)	−0.00080 (68)	0.01091 (29)
630^3	5.8934	5.89346 (34)	−0.00122 (68)	0.00607 (19)
636^3	5.8939	5.89324 (27)	−0.00165 (56)	0.00384 (15)
642^3	5.8940	5.89387 (20)	−0.00044 (44)	0.00241 (11)
648^3	5.8941	5.89366 (20)	−0.00084 (44)	0.00167 (10)
654^3	5.8941	5.89400 (10)	−0.00019 (28)	0.001159 (31)
660^3	5.8941	5.89447 (09)	+0.00071 (27)	0.000821 (24)
6∞	⋯	5.89410 (11)	0.00000 (21)	0
832^3	6.0615	6.06144 (64)	−0.0011(13)	0.01401 (61)
840^3	6.0616	6.06060 (53)	−0.0025(11)	0.00791 (40)
848^3	6.0620	6.06207 (44)	−0.00008 (99)	0.00470 (28)
856^3	6.0623	6.06201 (37)	−0.00018 (91)	0.00307 (23)
8∞	⋯	6.06212 (44)	0.00000 (67)	0.00470 (28)

TABLE II. PBC: Maxima (values at $\beta_{\max}$) of observables.

$N_\tau N_s^3$	$C_{\max}$	$\chi_{\max}$	$\chi^{\beta}_{\max}$	$F_{\max}$
$4\,12^3$	0.3848 (21)	3.61 (03)	0.1680 (15)	0.648 (05)
$4\,16^3$	0.5333 (41)	7.96 (10)	0.3303 (38)	1.030 (07)
$4\,20^3$	0.7557 (79)	15.32 (20)	0.5885 (81)	1.490 (13)
$4\,24^3$	1.102 (15)	27.95 (44)	1.013 (16)	2.009 (20)
$4\,28^3$	1.555 (17)	45.84 (54)	1.592 (22)	2.482 (22)
$4\,32^3$	2.142 (22)	70.37 (59)	2.365 (23)	2.993 (21)
$4\,36^3$	2.989 (30)	106.69 (96)	3.497 (45)	3.479 (29)
$4\,40^3$	4.103 (22)	154.34 (73)	4.984 (19)	3.977 (15)
$6\,24^3$	0.1552 (07)	5.08 (10)	0.063 (02)	0.984 (37)
$6\,30^3$	0.1696 (10)	9.12 (21)	0.103 (03)	1.35 (11)
$6\,36^3$	0.1866 (19)	14.83 (43)	0.154 (05)	1.869 (29)
$6\,42^3$	0.2143 (31)	24.22 (78)	0.238 (08)	2.349 (51)
$6\,48^3$	0.2443 (48)	35.4 (1.6)	0.332 (15)	2.789 (74)
$6\,54^3$	0.2866 (34)	52.5 (1.0)	0.475 (09)	3.412 (43)
$6\,60^3$	0.3464 (57)	76.7 (1.6)	0.674 (16)	4.176 (50)
$8\,32^3$	0.10834 (28)	3.14 (09)	0.0196 (06)	0.677 (16)
$8\,40^3$	0.11080 (37)	5.57 (21)	0.0310 (11)	0.938 (20)
$8\,48^3$	0.11466 (55)	9.68 (41)	0.0498 (25)	1.269 (30)
$8\,56^3$	0.11988 (78)	15.62 (83)	0.0737 (35)	1.702 (85)

is justified because there is only a little correlation between the β_t and β_t^∞ error bars. For $t = 0$ the error bar of the numerator of Eq. (23) is taken, keeping the denominator of the same β_t fixed. Whenever a comparison is possible, our estimates are statistically consistent with those by the Bielefeld group [24].

The last column of Table I gives the full width at $4/5$ maximum denoted by $\triangle\beta_t^{4/5}$. Due to the restricted range in which reweighting is possible, one is forced to use a height definition that is located unusually close to the maximum. Other results—the maxima of the specific heat (11), of the magnetic (13) and thermal (14) Polyakov loop susceptibilities, and of structure factors (15)—are collected in Table II. Their analysis is postponed to Sec. V.

IV. DECONFINING TRANSITION ON A DLT

In this section we report our DLT simulations. Our MCMC statistics per data point and our jackknife error analysis method are the same as in the previous section for PBC.

A. Pseudotransition temperatures

In Table III we collect our estimates of pseudotransition couplings β_t for $N_\tau = 4$, 6 and 8. For each N_τ, three reduced outside temperatures are used with their precise values listed in the table together with the corresponding β_{out} values from which they are derived via Eq. (23). For distinct temporal lattice sizes, the t_{out} values disagree slightly with the targeted values of Eq. (4). This is mainly due to a switch from the SU(3) lambda lattice scale of Ref. [20] to the better established one of Necco and Sommer [13]. To a minor extent, the differences are due to rounding of the β_{out} values.

TABLE III. DLT pseudotransition couplings.

		$\beta_{\text{out}} = 5.65$	$\beta_{\text{out}} = 5.66$	$\beta_{\text{out}} = 5.6767$
N_τ	N_s	$t_{\text{out}} = -0.0966$	$t_{\text{out}} = -0.0744$	$t_{\text{out}} = -0.0365$
4	12	5.72266 (28)	5.71509 (40)	5.70265 (36)
4	16	5.72224 (16)	5.71589 (28)	5.70332 (32)
4	20	5.71962 (14)	5.71481 (14)	5.70392 (24)
4	24	5.71557 (22)	5.71249 (18)	5.70424 (20)
4	28	5.71225 (18)	5.710104 (95)	5.70379 (15)
4	32	5.708855 (68)	5.707564 (74)	5.70315 (12)
4	36	5.706273 (99)	5.705415 (74)	5.702297 (92)
4	40	5.704364 (80)	5.703607 (83)	5.701417 (83)
		$\beta_{\text{out}} = 5.84318$	$\beta_{\text{out}} = 5.85514$	$\beta_{\text{out}} = 5.87514$
		$t_{\text{out}} = -0.0951$	$t_{\text{out}} = -0.0732$	$t_{\text{out}} = -0.0360$
6	24	5.93319 (35)	5.92418 (51)	5.90885 (64)
6	30	5.92846 (31)	5.92172 (25)	5.90937 (45)
6	36	5.92297 (31)	5.91905 (25)	5.90844 (21)
6	42	5.91816 (56)	5.91571 (26)	5.90777 (21)
6	48	5.91462 (26)	5.91289 (19)	5.90711 (24)
6	54	5.91136 (17)	5.91034 (13)	5.90622 (15)
6	60	5.90900 (13)	5.90802 (16)	5.90515 (20)
		$\beta_{\text{out}} = 6.004577$	$\beta_{\text{out}} = 6.018205$	$\beta_{\text{out}} = 6.040954$
		$t_{\text{out}} = -0.0923$	$t_{\text{out}} = -0.0708$	$t_{\text{out}} = -0.0344$
8	32	6.10827 (61)	6.09684 (97)	6.08005 (53)
8	40	6.10099 (46)	6.09550 (41)	6.08086 (50)
8	48	6.09549 (48)	6.09210 (40)	6.07938 (34)
8	56	6.09071 (28)	6.08752 (32)	6.07841 (24)
8	64	6.08647 (25)	6.08403 (33)	6.07735 (29)
8	72	6.08322 (29)	6.08103 (36)	6.07590 (20)

Because of the confined outside phase, the increase in the peaks of the Polyakov loop susceptibilities is for DLT BC less pronounced with lattice size than for PBC (finite-size scaling exponents are discussed in Sec. V). Iteration towards inside coupling constant values β_{in}, which include pseudotransition couplings β_t in their respective reweighting ranges, can be quite tedious. Instead of relying on a single final simulation, we often patch several simulations together using the approach of [23] for continuous variables. In the neighborhood of a maximum of the Polyakov loop susceptibility averages $\bar{\chi}_i$ from $i = 1, \ldots, p$ patches are combined with weights w_i to

$$\bar{\chi} = \sum_{i=1}^{p} w_i \bar{\chi}_i, \qquad \sum_{i=1}^{p} w_i = 1, \tag{24}$$

where the weights are up to a common constant proportional to the error bars of our estimators from individual patches,

$$w_i = \sim 1/\triangle\, \bar{\chi}_i. \tag{25}$$

For the error bar of the final estimator $\bar{\chi}$, the jackknife approach is applied to the entire sum (24). Limitations of the procedure are discussed in [23].

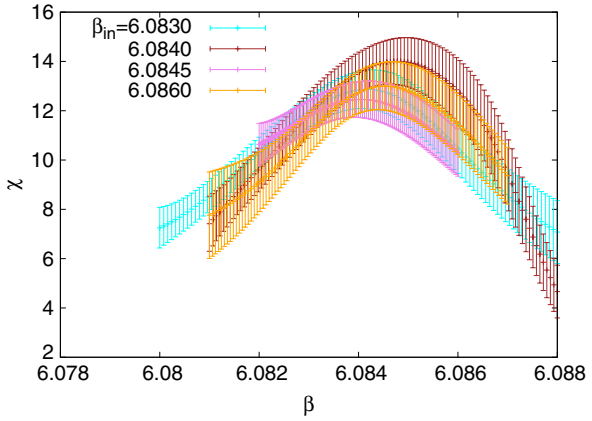

FIG. 2 (color online). Reweighting ranges of our final runs for the 864^3 DLT at $\beta_{\text{out}} = 6.018205$.

Figures 2 and 3 illustrate patching for one of our CPU time expensive simulations of an $8\,64^3$ DLT. All simulation points for the finally combined patches are listed in Tables IV and V. For $N_\tau = 8$, between one and five patches are used, for $N_\tau = 4$ and 6, between one and three are used. In the tables the numbers of patches are given in the columns headlined by p. In Table IV for the $N_\tau = 8$ lattices, we list in the third column the outside β values for each lattice size in increasing order. To fit the $N_\tau = 4$ and 6 information into one table, this information is omitted in Table V, but easily obtained from Table III as the simulation values for each lattice are given in the same order as employed in Table IV. Because first simulation points are always guessed on the basis of previous results, it depends a bit on chance how many patches are needed.

In Fig. 4 the β_t estimates for $N_\tau = 4$, 6 and 8 of Table III are plotted together, where at $N_\tau/N_s = 0$, i.e. for $N_s \to \infty$, the infinite volume extrapolations for PBC of Table I are taken as these results are not supposed to depend on BCs. The connecting lines are just to guide the eyes. It is obvious that there are large separations by lattice size, whereas the splits due to distinct outside temperatures are

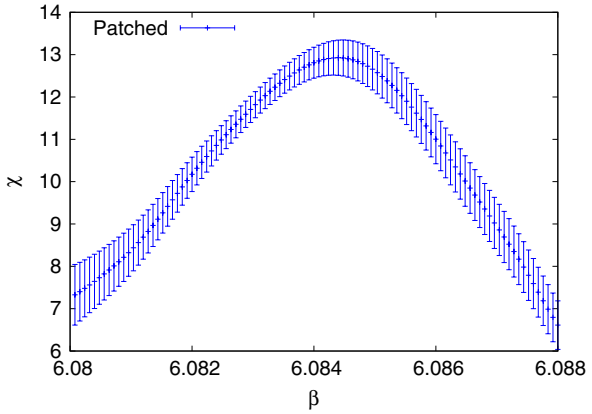

FIG. 3 (color online). Patching of the runs of the previous figure.

TABLE IV. DLT: $N_\tau = 8$ reweighting information.

N_s	p	β_{out}	β_1	β_2	β_3	β_4	β_5
32	3	6.004577	6.1075	6.1079	6.1090	⋯	
32	1	6.018205	6.0978	⋯	⋯	⋯	⋯
32	4	6.040954	6.0786	6.0800	6.0820	6.0850	⋯
40	4	6.004577	6.1008	6.1013	6.1018	6.1030	⋯
40	3	6.018205	6.0950	6.0960	6.0970	⋯	⋯
40	4	6.040954	6.0800	6.0805	6.0810	6.0815	⋯
48	3	6.004577	6.0950	6.0957	6.0980	⋯	⋯
48	2	6.018205	6.0927	6.0945	⋯	⋯	⋯
48	3	6.040954	6.0795	6.0803	6.0811	⋯	⋯
56	3	6.004577	6.0900	6.0910	6.0920	⋯	⋯
56	3	6.018205	6.0870	6.0875	6.0890	⋯	⋯
56	5	6.040954	6.0775	6.0779	6.0782	6.0791	6.0803
64	2	6.004577	6.0865	6.0885	⋯	⋯	⋯
64	4	6.018205	6.0830	6.0840	6.0845	6.0860	⋯
64	2	6.040954	6.0772	6.0775	⋯	⋯	⋯
72	2	6.004577	6.0829	6.0835	⋯	⋯	⋯
72	1	6.018205	6.0810	⋯	⋯	⋯	⋯
72	3	6.040954	6.0755	6.0760	6.0765	⋯	⋯

comparatively small (the larger β_t corresponding to the smaller β_{out} values). Applying relation (23) to translate our β_t into reduced temperatures $t = t(\beta_r)$, we arrive at Fig. 5. The dominant separation is now by β_{out} values with

TABLE V. DLT: $N_\tau = 4$ and $N_\tau = 6$ reweighting information. Rows with the same N_s/N_τ value are in the order of increasing β_{out}.

	$N_\tau = 4$				$N_\tau = 6$		
$\frac{N_s}{N_\tau}$	p	β_1	β_2	β_3	p	β_1	β_2	β_3
3	2	5.722	5.723	⋯				
3	1	5.7143	⋯	⋯				
3	1	5.7030	⋯	⋯				
4	3	5.7160	5.7180	5.7157	3	5.9250	5.9328	5.9343
4	1	5.7157	⋯	⋯	2	5.9250	5.9330	⋯
4	1	5.7040	⋯	⋯	1	5.9085	⋯	⋯
5	2	5.7180	5.7196	⋯	2	5.9280	5.9288	⋯
5	2	5.7140	5.7148	⋯	3	5.9205	5.9218	5.9241
5	1	5.7043	⋯	⋯	1	5.9091	⋯	⋯
6	1	5.7159	⋯	⋯	2	5.9230	5.9260	⋯
6	1	5.7125	⋯	⋯	2	5.9180	5.9189	⋯
6	1	5.7038	⋯	⋯	3	5.9082	5.9087	5.9094
7	1	5.7120	⋯	⋯	3	5.9175	5.9185	5.9190
7	2	5.7090	5.7100	⋯	2	5.9145	5.9160	⋯
7	1	5.7035	⋯	⋯	3	5.9076	5.9080	5.9094
8	3	5.7078	5.7090	5.7098	1	5.9150	⋯	⋯
8	2	5.7070	5.7075	⋯	3	5.9120	5.9130	5.9135
8	1	5.7030	⋯	⋯	3	5.9070	5.9076	5.9085
9	1	5.7060	⋯	⋯	2	5.9105	5.9115	⋯
9	2	5.7045	5.7055	⋯	3	5.9090	5.9103	5.9114
9	1	5.7022	⋯	⋯	2	5.9062	5.9078	⋯
10	2	5.7015	5.7045	⋯	3	5.9080	5.9090	5.9100
10	2	5.7033	5.7038	⋯	2	5.9070	5.9085	⋯
10	1	5.7012	⋯	⋯	1	5.9050	⋯	⋯

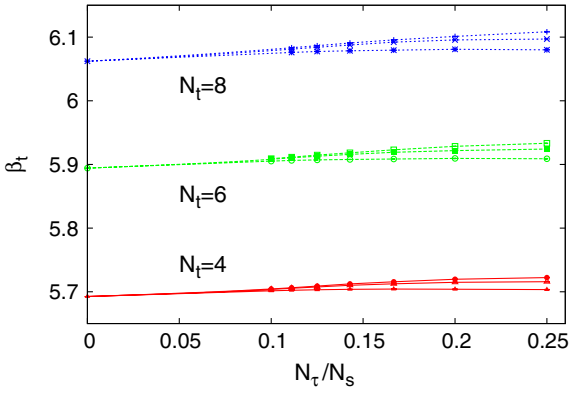

FIG. 4 (color online). DLT: Pseudotransition estimates β_t.

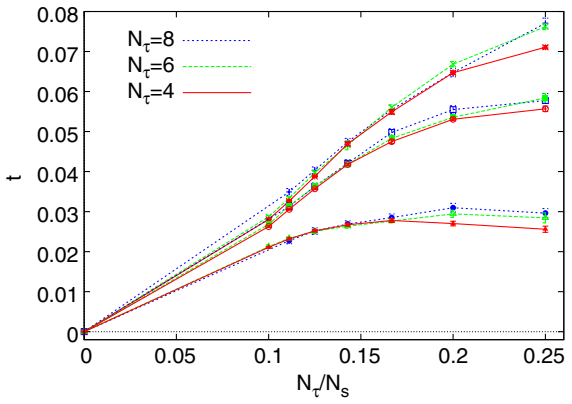

FIG. 5 (color online). DLT: Pseudotransition reduced temperature estimates $t = t(\beta_t)$.

different lattice sizes clustering due to scaling together. Scaling violations are visible, which increase towards small volumes (i.e., large N_τ/N_s).

We would like to extrapolate from our $N_\tau = 4$, 6, 8 results the finite volume continuum limit. This means

$$N_\tau \to \infty \quad \text{with} \quad x = \frac{L_\tau}{L_s} = \text{constant}. \tag{26}$$

While N_τ and N_s both approach infinity, the physical dimensions of the system, $L_\tau = aN_\tau$ and $L_s = aN_s$ with $a = a(\beta)$ lattice spacing, stay finite. Let us denote the data of Fig. 5 by $t(N_\tau, x)$. It is reasonable to assume for fixed outside temperature t_i, $i = 1$, 2, 3 that $t(N_\tau, x)$ can be expanded into a Taylor series of the variable $1/N_\tau$ about $t(\infty, x)$:

$$t(N_\tau; x) = t(\infty; x) + \frac{a_1(x)}{N_\tau} + \frac{a_2(x)}{(N_\tau)^2} + \frac{a_3(x)}{(N_\tau)^3} + \cdots.$$

For each fit there are three data points $N_\tau = 4$, 6 and 8 (with exception of $x = 0.1$ for which we have only $N_\tau = 4$ and 6). So, we are confined to the linear part of the expansion in $1/N_\tau$ and extract $t(\infty; x)$ from two parameter fits,

TABLE VI. To $N_\tau = \infty$ extrapolated reduced pseudotransition temperatures ($x = L_\tau/L_z$ (26)).

	t_1		t_2		t_3	
x	t	Q	t	Q	t	Q
0	0.0000 (06)	1	0.0000 (06)	1	0.0000 (06)	1
1/10	0.0300 (11)	⋯	0.0279 (12)	⋯	0.0216 (14)	⋯
1/9	0.0356 (11)	0.23	0.0326 (09)	0.67	0.0232 (10)	0.47
1/8	0.0417 (12)	0.84	0.0372 (11)	0.77	0.0249 (12)	0.90
1/7	0.0476 (16)	0.59	0.0421 (13)	0.81	0.0263 (12)	0.49
1/6	0.0571 (17)	0.46	0.0509 (14)	0.42	0.0282 (13)	0.42
1/5	0.0681 (15)	0.03	0.0560 (14)	0.19	0.0347 (19)	0.86
1/4	0.0850 (18)	0.32	0.0620 (26)	0.40	0.0338 (22)	0.92

$$t(N_\tau; x) = t(\infty; x) + \frac{a_1(x)}{N_\tau}. \tag{27}$$

The results for $t(\infty; x)$ are collected in Table VI together with each goodness of fit Q. In the overall picture, the Q values are quite satisfactory.

After we have thus estimated the finite volume continuum limit $t(\infty, x)$, we focus on the volume dependence of these estimates. As surface over volume varies $\sim 1/L_s$ and the temporal lattice dimension L_τ is kept fixed, we plot in Fig. 6 our $t(\infty, x)$ estimates as a function of $x = L_\tau/L_s$ together with fits of the form

$$t(\infty; x) = t(\infty, 0) + a_1 x. \tag{28}$$

For comparison we have also added $t(\infty, x)$ estimates from lattices with PBC, which give the essentially flat line at the bottom of the figure. For the three outside temperatures and PBC, the fit parameters are compiled in Table VII.

Towards large x we do not include our $t(\infty, x)$ estimates once they leave the straight line. Their turnaround contradicts the expectation that the influence of the confined outside phase increases in proportion to the surface over volume ratio. It is assumed to be an artifact due to our

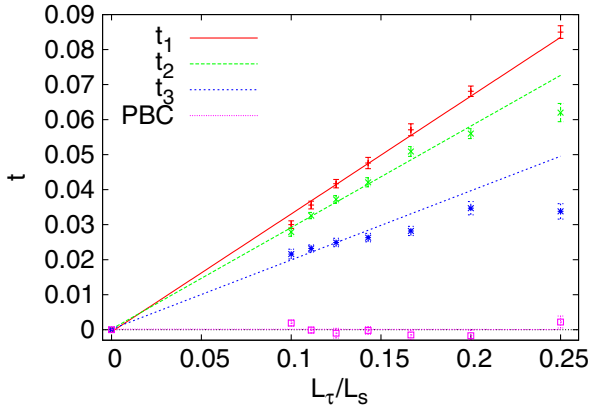

FIG. 6 (color online). Estimated behavior of reduced pseudotransition temperatures as function of the inverse spatial lattice extension L_τ/L_s with L_τ about 1.1 fm.

TABLE VII. Parameters obtained from fits to Eq. (28).

Outside	$t(\infty, 0)$	a_1	Q
t_1	−0.00059 (57)	0.3364 (51)	0.06
t_2	0.00005 (58)	0.2914 (54)	0.21
t_3	0.00018 (60)	0.1975 (69)	0.13
PBC	0.00014 (56)	−0.0003 (18)	0.18

choice of the DLT for implementing the BC. As outlined in [5], one can wind around each DLT layer along the diagonals. This leads to corner effects, where the inside phase connects with itself. Their importance appears to increase for smaller volumes and with decreasing temperature of the outside layer. Altogether, only four data points are omitted: None for outside temperature t_1 or PBC, the last (largest x) data point for t_2, and the last three for t_3. Their deviations from the straight line fits are clearly visible in Fig. 6. The somewhat small goodness of fit value $Q = 0.06$ for the t_1 fit is entirely due to the data point at $x = 0.1$ for which the $N_\tau = 8$ lattice was too big to be simulated ($Q = 0.63$ without this data point).

B. Width

In Table VIII we report our estimates of $\triangle\beta_t^{4/5}$, which are as in Sec. III C, the full width at $4/5$ of the maximum of the Polyakov loop susceptibility. After converting these values to reduced temperatures $\triangle t^{4/5}$, there are rather large scaling violations from $N_\tau = 4$ to $N_\tau = 6$, while the situation improves considerably from $N_\tau = 6$ to $N_\tau = 8$. For outside temperature t_3, this is illustrated in Fig. 7 (to guide the eyes, data points are connected by straight lines).

TABLE VIII. Widths $\triangle\beta_t^{4/5}$ of the magnetic Polyakov loop susceptibilities.

N_τ	N_s	$\beta_{\rm out} = 5.65$	$\beta_{\rm out} = 5.66$	$\beta_{\rm out} = 5.6767$
4	12	0.01767 (19)	0.01633 (24)	0.01563 (23)
4	16	0.00890 (11)	0.00805 (15)	0.00713 (15)
4	20	0.00539 (10)	0.00472 (08)	0.00379 (10)
4	24	0.00422 (16)	0.00323 (11)	0.002276 (56)
4	28	0.00335 (14)	0.002531 (78)	0.001498 (44)
4	32	0.002580 (71)	0.002185 (65)	0.001089 (44)
4	36	0.001986 (85)	0.001688 (64)	0.000869 (40)
4	40	0.001574 (69)	0.001319 (58)	0.000718 (38)
		$\beta_{\rm out} = 5.84318$	$\beta_{\rm out} = 5.85514$	$\beta_{\rm out} = 5.87514$
6	24	0.01458 (30)	0.01365 (42)	0.01191 (35)
6	30	0.00919 (26)	0.00837 (21)	0.00676 (24)
6	36	0.00674 (28)	0.00563 (19)	0.00419 (13)
6	42	0.00516 (23)	0.00462 (26)	0.00289 (11)
6	48	0.00402 (28)	0.00350 (16)	0.00197 (11)
6	54	0.00320 (17)	0.00278 (13)	0.00159 (14)
6	60	0.00250 (13)	0.00224 (15)	0.00131 (10)
		$\beta_{\rm out} = 6.004577$	$\beta_{\rm out} = 6.018205$	$\beta_{\rm out} = 6.040954$
8	32	0.01780 (43)	⋯	0.01471 (36)
8	40	0.01175 (39)	0.01008 (35)	0.00824 (32)
8	48	0.00882 (56)	0.00658 (47)	0.00540 (22)
8	56	0.00629 (58)	0.00484 (24)	0.00359 (13)
8	64	⋯	0.00422 (21)	0.00245 (17)
8	72	0.00365 (21)	0.00343 (39)	0.00202 (17)

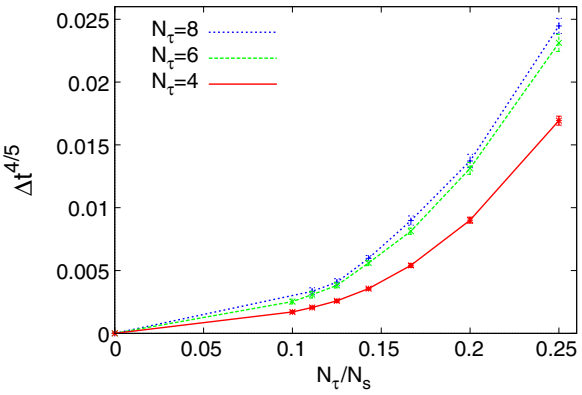

FIG. 7 (color online). Widths estimates for outside temperature t_3 and temporal lattice sizes $N_\tau = 4, 6, 8$.

We combine the widths, similarly as before the pseudo-transition temperatures using Eq. (27), and give the results in Table IX. When there are only $N_\tau = 4$ and 6 data points, there is no goodness of fit, as well as at $x = 0$, where the transition becomes sharp, so that the width is known to be zero.

For a first-order phase transition, the peaks of the Polyakov loop susceptibility develop δ-function singularities, i.e., the maxima increase proportionally to the spatial volume. Therefore, their widths decrease in leading order proportionally to x^3. However, fitting

$$\triangle t^{4/5} = a_1 x^3, \tag{29}$$

acceptable goodness-of-fit values are only obtained by restricting the fits to the smallest x values (corresponding to our largest $(N_s)^3$ volumes). To understand the effect better, we perform two-parameter fits of the form

TABLE IX. At fixed $x = L_\tau/L_s$ (26) to $N_\tau = \infty$ extrapolated widths. Power law parameters for fits to Eq. (30) are given in the last row.

	t_1		t_2		t_3	
x	$\triangle t_t^{4/5}$	Q	$\triangle t_t^{4/5}$	Q	$\triangle t_t^{4/5}$	Q
0	0.0 (0)	⋯	0.0 (0)	⋯	0.0 (0)	⋯
1/10	0.00707 (82)	⋯	0.00676 (92)	⋯	0.00419 (60)	⋯
1/9	0.00798 (63)	0.15	0.00796 (71)	0.61	0.00479 (48)	0.63
1/8	0.0112 (17)	⋯	0.00925 (60)	0.32	0.00586 (45)	0.39
1/7	0.0138 (13)	0.63	0.01110 (75)	0.01	0.00878 (39)	0.09
1/6	0.0195 (14)	0.96	0.0164 (11)	0.10	0.01303 (57)	0.34
1/5	0.0273 (11)	0.42	0.02440 (90)	0.20	0.01942 (91)	0.10
1/4	0.0407 (13)	0.50	0.0418 (26)	⋯	0.0328 (12)	0.14
⋯	a_2	Q	a_2	Q	a_2	Q
⋯	1.947 (74)	0.89	2.093 (94)	0.35	2.374 (72)	0.78

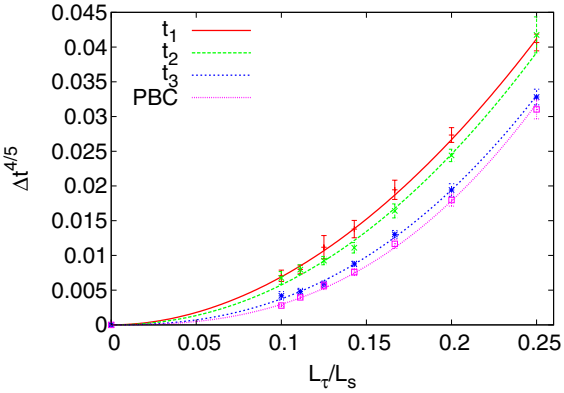

FIG. 8 (color online). Width estimates for $N_\tau = \infty$ and outside reduced temperatures t_1, t_2, t_3 as well as PBC. The lines are two-parameter fits (30) to the widths.

$$\triangle t^{4/5} = a_1 x^{a_2}, \tag{30}$$

which leave the exponent variable. Surprisingly, this allows us to fit all our width data consistently, as shown in Fig. 8. Together with the goodness of fit, the estimated exponents are given in the last row of Table IX. The pattern is that disorder (decreasing outside temperature) reduces the a_2 exponents, so that they look effectively like second-order phase transition exponents. Apparently, much larger lattices are needed to exhibit the weak first-order nature of the transition. This is even true for PBC, though the obtained effective exponent is the largest: $a_2 = 2.594\,(60)$ with $Q = 0.70$.

V. FINITE SIZE SCALING EXPONENTS

We consider the influence of DLT BCs with different outside temperatures on the finite-size scaling exponents of the specific heat C, the magnetic Polyakov loop susceptibility χ and the thermal Polyakov loop susceptibility χ^b. We extract estimates from the finite-size behavior of their maxima $C_{\max}$, $\chi_{\max}$ and $\chi^b_{\max}$ by performing two-parameter fits,

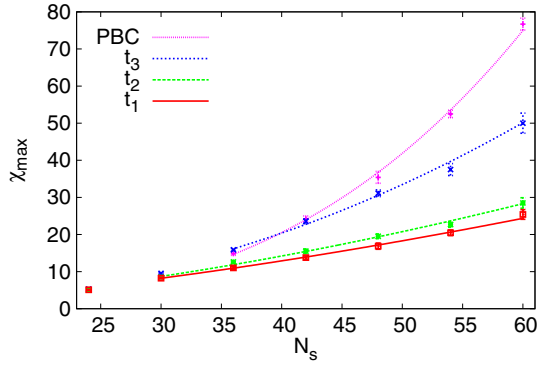

FIG. 9 (color online). Two-parameter exponent fits for the magnetic susceptibility $\chi_{\max}$ on $N_\tau = 6$ lattices.

$$Y(N_s) = a(N_s)^b. \tag{31}$$

Smaller lattices are omitted until an acceptable goodness of fit Q is obtained (this procedure avoids additional fit parameters for higher-order corrections, which tend to render such fits unstable).

For fixed N_τ and $N_s \to \infty$, one has to obtain the same exponents as with PBC, because we are still dealing with a weak first-order phase transition and the asymptotic behavior does not depend on the BC. However, effective estimates from our actual lattices show strong deviations from the asymptotic behavior. They are compiled in Table X, where n denotes the number of data points used

TABLE X. Estimates of finite-size scaling exponents from two-parameter fits (31) for our data with DLT BC and PBC.

	$C_{\max}$			$\chi_{\max}$			$\chi^b_{\max}$		
	b	Q	n	b	Q	n	b	Q	n
	$N_\tau = 4$			$N_\tau = 4$			$N_\tau = 4$		
t_1	0.776 (80)	0.97	4	1.381 (36)	0.33	6	1.163 (70)	0.30	5
t_2	0.83 (15)	0.73	3	1.75 (18)	0.73	3	1.52 (26)	0.67	3
t_3	1.27 (11)	0.24	4	2.01 (11)	0.29	4	1.70 (13)	0.26	4
PBC	2.925 (51)	0.39	3	3.441 (30)	0.16	4	3.343 (46)	0.86	3
	$N_\tau = 6$			$N_\tau = 6$			$N_\tau = 6$		
t_1	0.242 (09)	0.83	7	1.569 (55)	0.91	6	1.198 (58)	0.91	6
t_2	0.275 (09)	0.57	7	1.702 (48)	0.05	6	1.323 (49)	0.10	6
t_3	0.591 (21)	0.86	6	2.219 (83)	0.20	5	2.173 (40)	0.13	7
PBC	1.58 (12)	0.16	3	3.195 (64)	0.36	5	2.863 (70)	0.31	5
	$N_\tau = 8$			$N_\tau = 8$			$N_\tau = 8$		
t_1	0.0898 (38)	0.26	6	1.537 (77)	0.12	5	1.220 (55)	0.11	6
t_2	0.1074 (55)	0.39	6	1.637 (95)	0.69	5	1.279 (77)	0.18	5
t_3	0.1956 (94)	0.20	5	2.637 (70)	0.51	6	2.215 (47)	0.69	6
PBC	0.222 (20)	0.17	3	2.824 (92)	0.36	4	2.345 (93)	0.29	4

TABLE XI. DLT: Maxima $\chi_{\max}$ of the Polyakov loop susceptibility (values at $\beta_{\max}$).

N_τ	N_s	$\beta_{\rm out} = 5.65$	$\beta_{\rm out} = 5.66$	$\beta_{\rm out} = 5.6767$
4	12	3.67 (03)	3.75 (04)	3.63 (04)
4	16	7.58 (07)	8.01 (11)	8.27 (13)
4	20	12.56 (17)	13.90 (17)	16.20 (30)
4	24	15.81 (41)	20.25 (49)	27.89 (50)
4	28	19.09 (54)	25.47 (57)	42.80 (92)
4	32	23.54 (46)	28.31 (61)	58.9 (1.8)
4	36	28.42 (86)	34.49 (93)	72.4 (2.4)
4	40	33.8 (1.1)	42.1 (1.5)	86.4 (3.3)
		$\beta_{\rm out} = 5.84318$	$\beta_{\rm out} = 5.85514$	$\beta_{\rm out} = 5.87514$
6	24	5.11 (08)	5.04 (11)	5.30 (11)
6	30	8.23 (17)	8.51 (15)	9.53 (24)
6	36	11.00 (34)	12.60 (30)	15.86 (35)
6	42	13.77 (43)	15.51 (60)	23.58 (64)
6	48	16.86 (83)	19.52 (63)	31.12 (90)
6	54	20.47 (75)	22.68 (73)	37.5 (1.6)
6	60	25.4 (1.3)	28.5 (1.4)	50.0 (2.7)
		$\beta_{\rm out} = 6.004577$	$\beta_{\rm out} = 6.018205$	$\beta_{\rm out} = 6.040954$
8	32	3.556 (69)	3.27 (11)	3.35 (12)
8	40	5.39 (13)	5.98 (13)	6.43 (17)
8	48	7.14 (24)	8.46 (39)	10.27 (31)
8	56	9.30 (31)	10.48 (68)	14.98 (87)
8	64	9.41 (71)	12.46 (74)	21.7 (1.2)
8	72	13.65 (63)	16.1 (1.3)	27.5 (2.1)

and refers always to the largest available lattices (see, e.g., Table III for a list of all simulated DLT lattices).

Instead of the predicted (20) first-order exponent $b = D = 3$, far smaller values are obtained. With N_τ fixed the systematic trend is that the exponents for outside temperature t_3 are larger than those for t_1 and t_2. To give an example, we show in Fig. 9 the fits of the maxima of the magnetic susceptibility for $N_\tau = 6$ lattices.

The used $\chi_{\max}$ data are compiled in Table XI, and the other maxima can be found in [17]. One may assume that larger N_τ values need also larger spatial lattice sizes N_s to exhibit asymptotic behavior. Our data take care of this by keeping N_s/N_τ for all N_τ in the same range. Nevertheless, the scaling behavior of the specific heat is for $N_\tau = 8$ in all cases, including PBC, erratic: The $C(\beta)$ curves show only very broad peaks. They are expected to sharpen for even larger N_s, but those are beyond our computational means.

VI. SUMMARY AND CONCLUSIONS

Our simulations show that even for relatively small temperature differences between outside and inside volumes, sizeable small volume corrections survive for pseudotransition temperatures. Using the illustrative scale of the Introduction, the volume dependence of our present estimates from PBC and DLT calculations, together with those from CBCs [4], are shown in Fig. 10 for L_s^3 volumes with

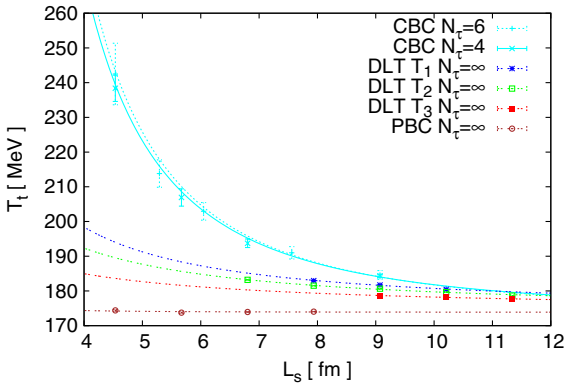

FIG. 10 (color online). Small volume corrections for the pseudotransition temperature with CBC, DLT and PBC boundaries.

edge length L_s between 4 and 12 fm. With PBC there are practically no finite-size corrections. Then, pseudotransition temperatures increase when the outside temperature falls below the infinite volume deconfining transition temperature. For the outside temperatures used in this paper, the change is less pronounced than with CBCs, but astonishingly large when one bears in mind that CBCs are supposed to model zero outside temperature and that our DLT BCs are only moving up to 10% in this direction on the scale of the transition temperature. This suggests that CBC estimates are realistic and not just a strong coupling artifact.

While a lot of work has focused on including quarks, little has so far been done about calculating small volume corrections, which increase the SU(3) transition temperature, while quark effects decrease it. The SU(3) simulations suggest that the magnitudes of the changes are similar. Assuming that the increase with decreasing volume holds also with quarks included, lattice calculations with PBC would underestimate the pseudotransition temperature in RHIC. The width of the transition is broadened by both effects, so that the conversion into a crossover is expected to become even more eminent. See Fig. 8 for the width estimates of this paper.

Including quarks requires building on software of one of the large scale QCD collaborations. At least in the first stage, one should fall back to simple CBCs as one cannot afford a multiplicative CPU time increase due to more involved BCs and fermions. This limitation appears acceptable, as our SU(3) DLT calculations support the relevance of the earlier CBC estimates. CBC modifications of, e.g., the MILC code would already be laborious, because to reduce discretization errors one has to implement CBCs for improved actions like [25] in both gauge and fermionic sectors.

A supporting investigation could aim at a further perfection of the BC between cold and hot regions of pure SU(3) gauge theory. This should include studying the effect due to a cold surrounding geometry instead of a DLT. Using the always confined [26] spacelike string tension as an additional scale would allow one to tune

couplings for spacelike and timelike plaquettes distinctly, so that the space transition from deconfined to confined volumes becomes entirely smooth.

ACKNOWLEDGMENTS

This work was supported in part by the U.S. Department of Energy under Contracts No. DE-FA02-97ER41022 and No. DE-FG02-13ER41942. In addition, we received generous CPU time support form the National Energy Research Scientific Computing Center (NERSC), and our data were generated under NERSC Energy Research Computing Allocations Process (ERCAP) Requests No. 84866, No. 84861, No. 84795, No. 84105, No. 85832 and No. 85833.

[1] J. M. Blatt and V. F. Weisskopf, *Theoretical Nuclear Physics* (Wiley, New York, 1952).
[2] P. F. Kolb and U. W. Heinz, in *Quark Gluon Plasma 3*, edited by R. C. Hwa and X. N. Wang (World Scientific, Singapore, 2003), p. 634.
[3] C. Spieles, H. Stocker, and C. Greiner, Phys. Rev. C **57**, 908 (1998); A. Gopie and M. C. Ogilvie, Phys. Rev. D **59**, 034009 (1999); L. M. Abreu, M. Gomes, and A. J. da Silva, Phys. Lett. B **642**, 551 (2006).
[4] A. Bazavov and B. A. Berg, Phys. Rev. D **76**, 014502 (2007).
[5] B. A. Berg, A. Bazavov, and H. Wu, Proc. Sci., LAT2009 (2009) 164 [arXiv:0909.3077].
[6] N. Yamamoto and T. Kanazawa, Phys. Rev. Lett. **103**, 032001 (2009).
[7] L. F. Palhares, E. S. Fraga, and T. Kodama, J. Phys. G **37**, 094031 (2010); **38**, 085101 (2011); E. S. Fraga, L. F. Palhares, and P. Sorensen, Phys. Rev. C **84**, 011903(R) (2011).
[8] J. Braun, B. Klein, H. J. Pirner, and A. H. Rezaeian, Phys. Rev. D **73**, 074010 (2006); J. Braun, B. Klein, and B.-J. Schaefer, Phys. Lett. B **713**, 216 (2012).
[9] A. Bhattacharyya, P. Deb, S. K. Ghosh, R. Ray, and S. Sur, Phys. Rev. D **87**, 054009 (2013).
[10] L. Levkova, Proc. Sci., Lattice (2011) 011 [arXiv:1201.1510].
[11] K. G. Wilson, Phys. Rev. D **10**, 2445 (1974).
[12] M. Fukugita, M. Okawa, and A. Ukawa, Nucl. Phys. **B337**, 181 (1990) and references given therein.
[13] S. Necco and R. Sommer, Nucl. Phys. **B622**, 328 (2002).
[14] B. A. Berg and H. Wu, Comput. Phys. Commun. **183**, 2145 (2012).
[15] H. J. Rothe, *Lattice Gauge Theories: An Introduction* (World Scientific, Singapore, 2005), 4th ed.
[16] B. A. Berg, *Markov Chain Monte Carlo Simulations and Their Statistical Analysis* (World Scientific, Singapore, 2004).
[17] H. Wu, Ph.D. thesis, Florida State University, 2012.
[18] G. Parisi, R. Petronzio, and F. Rapuano, Phys. Lett. **128B**, 418 (1983).
[19] H. E. Stanley, *Introduction to Phase Transitions and Critical Phenomena* (Clarendon Press, Oxford, 1971), p. 98.
[20] A. Bazavov, B. A. Berg, and A. Velytsky, Phys. Rev. D **74**, 014501 (2006).
[21] A. Pelissetto and E. Vicari, Phys. Rep. **368**, 549 (2002).
[22] A. M. Ferrenberg and R. H. Swendsen, Phys. Rev. Lett. **61**, 2635 (1988); **63**, 1658 (1989) and references therein.
[23] N. A. Alves, B. A. Berg, and S. Sanielevici, Nucl. Phys. **B376**, 218 (1992).
[24] G. Boyd, J. Engels, F. Karsch, E. Laermann, C. Legeland, M. Lütgemeier, and B. Peterson, Nucl. Phys. **B469**, 419 (1996).
[25] A. Bazavov *et al.*, Rev. Mod. Phys. **82**, 1349 (2010); A. Bazavov and P. Petreczky, J. Phys. G **38**, 124099 (2011).
[26] O. Andreev, Phys. Lett. B **659**, 416 (2008) and references therein.